



# Efficient white LEDs with bright green-emitting CsPbBr<sub>3</sub> perovskite nanocrystal in mesoporous silica nanoparticles



Xiaoxuan Di, Ludi Shen, Jutao Jiang, Meiling He, Yinzi Cheng, Lei Zhou, Xiaojuan Liang<sup>\*</sup>, Weidong Xiang<sup>\*\*</sup>

College of Chemistry and Materials Engineering, Wenzhou University, Wenzhou, Zhejiang, 325035, China

## ARTICLE INFO

### Article history:

Received 30 July 2017

Received in revised form

19 September 2017

Accepted 20 September 2017

Available online 21 September 2017

### Keywords:

CsPbBr<sub>3</sub> NCs

NCs-MS

Optical performance

Luminous efficacy

White light-emitting diode

## ABSTRACT

Metal-halide perovskites have been hailed as remarkable materials for photovoltaic devices and, recently, their star has also been on the rise in optoelectronics and photonics. Nevertheless, challenging issues, such as the thermal/chemical stability and high-performance devices with long-term stability, limit their practical applications. Here, we successfully prepared CsPbBr<sub>3</sub> NCs incorporated into mesoporous silica (NCs-MS) by a simple stirred of MS with CsPbBr<sub>3</sub> NCs blended in toluene solution. The resultant NCs-MS nanocomposite exhibit excellent optical performance and good thermal and photostability under illumination of UV light for 120 h. Additionally, NCs-MS nanocomposite is resistant to water, which are beneficial for the fabrication of white light-emitting diode (WLED) devices. Thereby a WLED was constructed by combining NCs-MS nanocomposite with Sr<sub>2</sub>Si<sub>5</sub>N<sub>8</sub>:Eu<sup>2+</sup> red phosphor on an InGaN blue chip, achieving a highly efficient luminous efficacy of 47.6 lm/W. Moreover, the WLED also demonstrate wonderful color stability under 120 mA current. This work opens up the exciting opportunity of using all-inorganic CsPbBr<sub>3</sub> NCs-MS nanocomposite for high performance and low-cost WLEDs applications.

© 2017 Elsevier B.V. All rights reserved.

## 1. Introduction

Metal-halide perovskites with a crystal structure of ABX<sub>3</sub>, where A is a monovalent cation (Cs<sup>+</sup>, CH<sub>3</sub>NH<sub>3</sub><sup>+</sup> or (NH<sub>2</sub>)<sub>2</sub>CH<sup>+</sup>) and B is an inorganic metal cation (Pb<sup>2+</sup> or Sn<sup>2+</sup>) in an octahedral coordination with six halide anions X (X = Cl, Br or I), have been extensively studied [1–8]. Over the past years, hybrid organic-inorganic lead halide perovskites, i.e., CH<sub>3</sub>NH<sub>3</sub>PbX<sub>3</sub> (X = Cl, Br, and I), have been intensively explored as promising photovoltaic materials and a respectable certified power conversion efficiency exceeding 22% has been achieved so far. More importantly, all-inorganic perovskite NCs (CsPbX<sub>3</sub> NCs with X = Br, I, Cl) have emerged as a new class of semiconductor NCs with remarkable optical properties, impressive high quantum yields (QYs), narrow full width at half maximums (FWHMs), and with huge promise in NC-based photovoltaics, light-emitting diodes (LED), and lasing applications [9–17]. Their emission lights not only cover the entire visible

spectra region and can be easily adjusted by controlling their composition and crystal size, but also their synthesis can be done with much lower temperatures and simpler procedures that are more facile and precise than cadmium chalcogenide based NCs [18,19]. Song et al. demonstrated LEDs of different colors based on CsPbX<sub>3</sub> (X = Cl, Br or I) NCs, while Zhang and co-workers recently reported the improved brightness of CsPbBr<sub>3</sub> NCs based green LEDs by introducing a thin layer of perfluorinated ionomer in between the hole transporting layer and the light-emitting perovskite layer [12,20].

In spite of their outstanding optical performance and high QYs, several challenging issue, such as the easy degradation under humid conditions and the thermal/moisture stability. From a practical viewpoint, when NCs are exposed to an external source of energy for a long time, several factors such as humidity, light, temperature, and oxygen, can induce the degradation. This is critical for practical photoelectronic applications, where long-term stability and cost-effectiveness are crucial [21–24]. Currently, significant ongoing research efforts have been devoted to improve the stability. For example, Pan et al. have demonstrated stability in air at high optical fluence for more than one day by passivating their surface with di(dodecyl)dimethylammonium sulfide [25], while the Manna's group employed X-ray irradiation to treat NCs, thus caused

<sup>\*</sup> Corresponding author.

<sup>\*\*</sup> Corresponding author.

E-mail addresses: [lxj6126@126.com](mailto:lxj6126@126.com) (X. Liang), [xiangweidong001@126.com](mailto:xiangweidong001@126.com) (W. Xiang).

intermolecular C=C bonding of the organic ligands that coated on the NCs surface to enhance the stability in air [26]. Additionally,  $\text{Mn}^{2+}:\text{CsPbCl}_3/\text{CsPbBr}_3$  NCs,  $\text{CsPbX}_3/\text{ZnS}$  NCs heterostructure, and phosphonic acid stabilized  $\text{CsPbX}_3$  NCs were reported, wherein the stability of NCs was significantly improved [27,28]. To the best of our knowledge, most inorganic matrix materials are mechanically robust and airtight. Among them  $\text{SiO}_2$  often are used as protection materials to protect phosphors, and metals from oxidations, corrosions or other chemical attacks owing to the very low diffusion rates. The inert silica encapsulation has a great potential to solve the stability and toxicity issues of NCs as the layer would block both the penetration of reactive oxygen and water to the NCs surface and the release of toxic heavy metal ions into the environment. Furthermore,  $\text{SiO}_2$  is feasible to transfer various types of hydrophobic NCs into aqueous solution or change their surface functionality to meet specific requirements for real applications [29]. Therefore, many interesting properties have been reported in this material, such as Zhang et al. used organosilicon (3-aminopropyl) triethoxysilane (APTES) as capping agent to synthesize QDs/silica composites by the hydrolysis [30]. In addition, Huang and co-workers utilized surface protection of NCs with polyhedral oligomeric silsesquioxane (POSS) [31]. Nevertheless, both methods achieved lower improvements in the stability of the QDs, particularly the thermal stability. No available QDs have yielded high-performance devices with long-term stability. It is, hence, imperative to develop an efficient and stable approach that improves the stability of NCs to fabricate high-performance LEDs. And endow NCs material immune to degradation, in particular, by moisture, such that long-term device stability can be attained.

Herein, we successfully incorporated  $\text{CsPbBr}_3$  NCs into mesoporous silica (NCs-MS) with a non-chemical process in toluene, and obtained an excellent luminescent NCs-MS nanocomposite with remarkable optical performance and high stability in humidity environment. It is worth to note that the PL QY of the NCs-MS nanocomposite was mostly preserved as 46% and did not have huge change after 120 h. For the first time, a white LED (WLED) was constructed by mixing the as-prepared green-emitting NCs-MS nanocomposite and red-emitting  $\text{Sr}_2\text{Si}_5\text{N}_8:\text{Eu}^{2+}$  red phosphors with promising performance at a driving current of 20 mA, as well as high long-term stability. NCs-MS nanocomposite have shown great potentials to practically utilize NCs in LED device with high efficiency and stability for lighting as well as displays.

## 2. Experimental

### 2.1. Materials

All the chemicals were used without further purification, cesium carbonate ( $\text{Cs}_2\text{CO}_3$ , 99.9%), lead bromide ( $\text{PbBr}_2$ , 98%), oleic acid (OA, 90%), oleylamine (OAm, 90%), 1-octadecene (ODE, 90%), toluene (98%), mesoporous silica (99.5%) were purchased from Aladdin.

### 2.2. Synthesis of $\text{CsPbBr}_3$ NCs

0.814 g  $\text{Cs}_2\text{CO}_3$ , 30 mL ODE, 2.5 mL OA were added into a 100 mL 3-neck flask, dried and heated to 120 °C under  $\text{N}_2$  for 1 h. Then further heated to 150 °C until a clear solution was observed. Then 10 mL ODE, 0.376 mmol  $\text{PbBr}_2$ , 0.6 mL OA and 0.6 mL OAm were loaded into a 50 mL 3-neck flask, dried under vacuum for 1 h at 120 °C, then switch to  $\text{N}_2$  protection until solution became clear. Afterward, the temperature was increase to 180 °C and 0.8 mL Cs-oleate solution (preheated to 100 °C) was injected into the as-prepared solution. After 5s later, the 3-neck flask was placed in an ice-water bath and cooled to room temperature. The crude

solution was centrifuged at 8000 rpm for 10 min, and then the precipitate was dispersed in toluene solution. One more centrifugation was required for purifying the final NCs.

### 2.3. Coating of $\text{CsPbBr}_3$ NCs with mesoporous silica nanocomposite (NCs-MS)

The preparation was performed by mixing the  $\text{CsPbBr}_3$  NCs toluene solution with mesoporous silica in a 3-neck flask. The solution was stirred for 1 h under  $\text{N}_2$  protection. Afterward, the precipitate was obtained by centrifugation at 5000 rpm for 10 min, then the precipitate was dried at 40 °C for 30 min under vacuum (Fig. 1).

### 2.4. Fabrication of WLEDs

To investigated the potential of NCs-MS nanocomposite applications in WLEDs, the as-prepared green-emitting NCs-MS nanocomposite,  $\text{Sr}_2\text{Si}_5\text{N}_8:\text{Eu}^{2+}$  red phosphors and silica gel (gel A:gel B = 1:1) were mixed in 20 mL beaker to obtain a homogeneous latex. Finally, the WLEDs was fabricated by combining the latex with blue-emitting InGaN chip and then dried in a vacuum oven at 50 °C. Note that the optical performance of the as-prepared WLEDs can be tuned by changing the relative proportion of NCs-MS nanocomposite and phosphor, and the coating volume of NCs-MS/phosphor silicone gel.

### 2.5. Characterizations

The structure and phase purity of the as-fabricated NCs in solution and NCs-MS nanocomposite were confirmed by X-ray diffraction (XRD, D8 Advance, Bruker, Germany) with Cu  $K\alpha$  radiation operated at 40 kV and 40 mA. To realize the microstructure of NCs in solution and the distribution of particles size, transmission electron microscopy (TEM) and high-resolution TEM (HRTEM) images were obtained using FEI Tecnai F20 operating at 200 kV. To further realize the surface structures of the sample, X-ray photoelectron spectroscopy (XPS) analysis was collected using an Axi Ultra DLD spectrometer with monochromatic Al  $K\alpha$  as the excitation source. The photoluminescence (PL), PL quantum efficiency (QY) and temperature-dependent emission spectra of the samples were gained on a spectrofluorometer (Edinburgh, FS5) equipped with both continuous (150 W) and pulsed xenon lamps. The decay curves of the samples were obtained using a spectrofluorometer (Edinburgh, FLS920) equipped with a 460 nm pulsed diode laser (EI-EPL-460). Optical properties of WLEDs such as the luminous efficacy, chromaticity coordinates, color rendering index, and correlated color temperature were measured using an integrating sphere (PMS-50, Everfine, China) under a forward current of 20 mA.

## 3. Results and discussion

The prepared all-inorganic perovskite  $\text{CsPbBr}_3$  NCs was investigated using the transmission electron microscopy (TEM) as illustrated in Fig. 2. It can be seen that  $\text{CsPbBr}_3$  NCs has a uniform nanocube morphology and a high crystallinity with perovskite structure (Fig. 2b). In addition, NCs has a size around 13 nm (Fig. 2a and inset), and the size of the NCs was beyond the calculated Bohr exciton diameter of  $\text{CsPbBr}_3$  (~7 nm) [32], which indicate a weak quantum confinement effect for our  $\text{CsPbBr}_3$  NCs. The calculated optical band gap of  $\text{CsPbBr}_3$  NCs is about 2.4 eV. According to the UV-vis absorption spectra (Fig. 5a), which is quite close to the previously reported value of 2.3 eV for  $\text{CsPbBr}_3$  single crystals [33]. It should be mentioned that the corresponding high-resolution TEM (HRTEM) image was presented in Fig. 2c. The interplanar

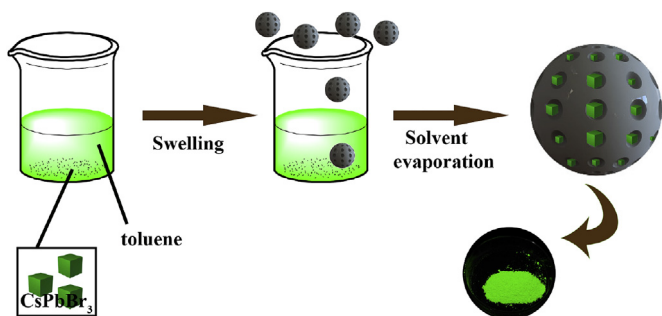


Fig. 1. Schematic illustration of formation of NCs-MS nanocomposite.

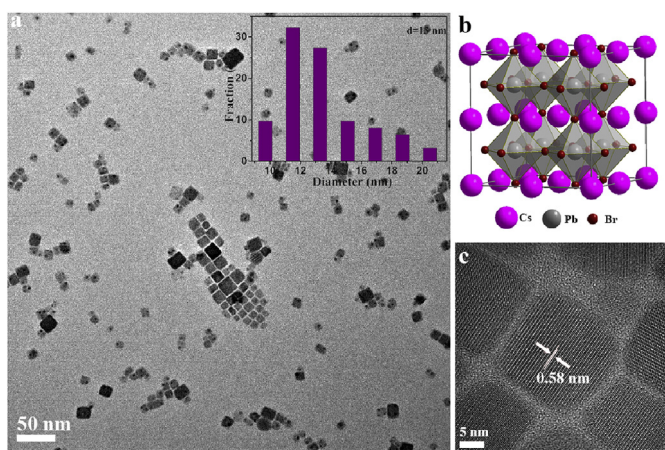


Fig. 2. (a) TEM micrograph of the CsPbBr<sub>3</sub> NCs; inset shows the size distribution of CsPbBr<sub>3</sub> NCs, (b) Schematic illustration of the perovskite cubic crystal structure, (c) HRTEM image of CsPbBr<sub>3</sub> NCs.

distance were measured to be around 0.58 nm, which is corresponding to the (100) crystal plane of the cubic perovskite CsPbBr<sub>3</sub> NCs (PDF#54-0752). Based on the abovementioned results, we concluded that CsPbBr<sub>3</sub> NCs have a very good crystallinity, which is preferred for improving the luminescence efficiency and the LED device performance.

Generally, CsPbX<sub>3</sub> are known to crystallize in orthorhombic, tetragonal, and cubic polymorphs of the perovskite lattice with the cubic phase being the high-temperature state for all compounds

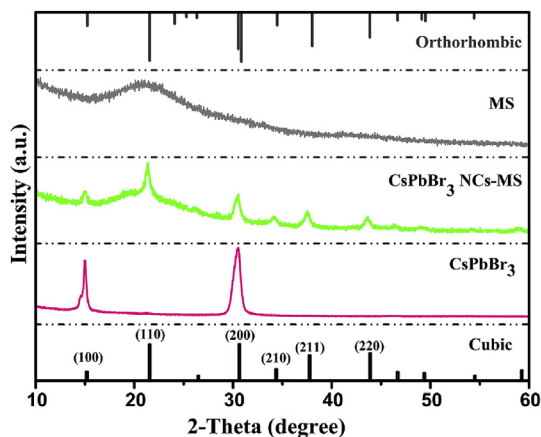


Fig. 3. XRD patterns of CsPbBr<sub>3</sub> NCs, MS treated CsPbBr<sub>3</sub> NCs, and the MS. The top and bottom pattern is the standard XRD pattern of orthorhombic and cubic phase CsPbBr<sub>3</sub>.

[4]. In our work, we find that the CsPbBr<sub>3</sub> NCs crystallize in the cubic phase (Fig. 3), which can be owing to the combined effect of high synthesis temperature and contributions from the surface energy. Fig. 3 shows the X-ray diffraction (XRD) pattern of the solid film of CsPbBr<sub>3</sub> NCs, which was fabricated using the spin-casting method to deposit the solution of as-synthesized CsPbBr<sub>3</sub> NCs on the upper surface of the quartz substrates, the as-prepared MS treated CsPbBr<sub>3</sub> NCs (NCs-MS) and the pure MS. As can be seen, the CsPbBr<sub>3</sub> NCs exhibited a cubic perovskite structure (PDF#54-0752), but only the (100) and (200) diffraction peaks of the cubic perovskite structure were obtained, indicating the sample exhibited preferential assembly along (100) and (200) planes during the film-forming process [24]. But differs from Ref. [17] that suggested orthorhombic phase for CsPbBr<sub>3</sub> NCs. In contrast, the sample of the as-prepared NCs-MS nanocomposite showed that the diffraction peaks with the 2-Theta values located at 15.01°, 21.2°, 30.4°, and 37.6° are consistent well with the (100), (110), (220), and (211) planes of the standard cubic CsPbBr<sub>3</sub> (PDF#54-0752). The pure MS has one broad peak corresponding to its amorphous structure, which is similar to other reports [4]. At the same time, a broad peak around 20°–25° was also observed in the NCs-MS nanocomposite sample, which was possibly owing to the amorphous structure of MS. An X-ray photoelectron spectroscopy (XPS) result of the NCs-MS nanocomposite was also analyzed. As shown in Fig. 4a and d, the main peaks of Cs 3d, Pb 4f and Br 3d have the similar binding energies compared to the NCs reported by other groups [34,35]. To further confirm the chemical bond configuration of the element, the bonding states of Br was investigated. As shown in Fig. 4d, the Br 3d peaks can be fitted into two peaks (3d<sub>5/2</sub>, 3d<sub>3/2</sub>) with binding energies of 67.9 and 68.3 eV, respectively, which correspond to the inner and surface ions. It worth noting that the position and the shape of main peak for Si 2p from the NCs-MS nanocomposite are nearly the same to other report [30], indicating the SiO<sub>2</sub> is well dispersed in the nanocomposite.

To better understand the fluorescence properties, we studied the PL emission and absorption spectra of NCs solution and as-prepared NCs-MS nanocomposite, as shown in Fig. 5a and inset, respectively. As we can see, NCs solution and NCs-MS nanocomposite all showed a very strong green fluorescence under UV excitation (365 nm). Absorption spectra of NCs-MS nanocomposite did not change much compared to the solution. However, the PL emission wavelength of NCs-MS nanocomposite was shifted approximately 3 nm from 518 nm to 521 nm, which is owing to the enlarged particle size. It is worth to note that little variation of the full width at half-maximum (FWHM) (25 nm for NCs-MS nanocomposite) was seen due to the Ostwald ripening. The existence of defect related states in the gap between the valance band and the conduction band will capture electrons from the conduction band, from which the defect-related emitting states will be detected. The independence of the position and shape of the NCs-MS nanocomposite emission band on the excitation wavelengths ranging from 365 to 500 nm indicates the absence of the defect-related emitting states for the present sample (Fig. 5b). Furthermore, the time-solved decay spectra of the NCs-MS nanocomposite and solution are shown in Fig. 5d, The PL decay spectra can be fitted by a second order exponential formula, and the two-component decay model is described as below:

$$F(t) = \sum a_i e^{-(t-t_0)/\tau_i} \quad i = 1, 2 \quad (1)$$

where  $a_i$  is a prefactor and  $\tau_i$  is the excited-state fluorescence lifetime associated with the  $i$ th component. As we can see that the PL decay lifetimes were 13.6 (for NCs solution) and 10.2 ns (for NCs-MS nanocomposite), respectively, which are similar to other works

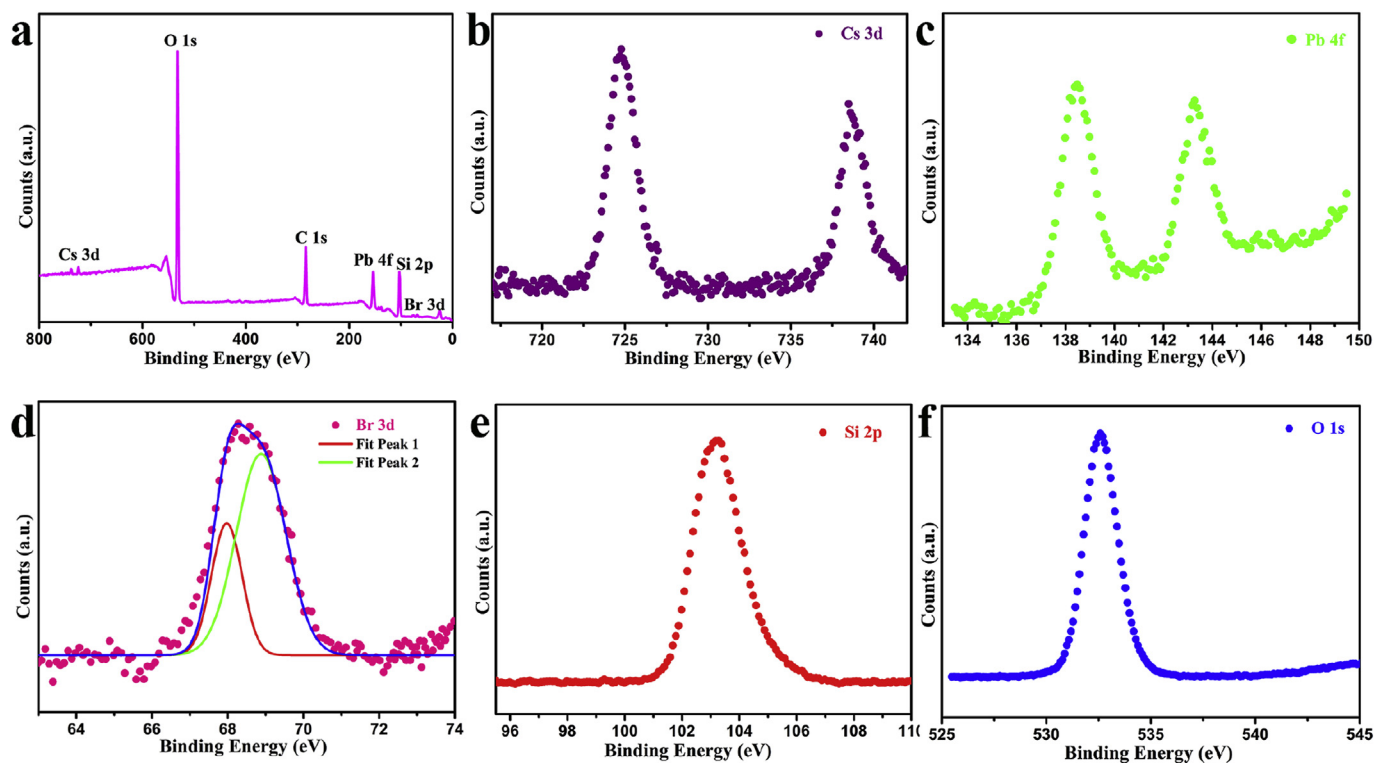


Fig. 4. (a) XPS spectra of NCs-MS nanocomposite, high resolution spectra of (b) Cs 3d, (c) Pb 4f, (d) Br 3d, (e) Si 2p, (f) O 1s.

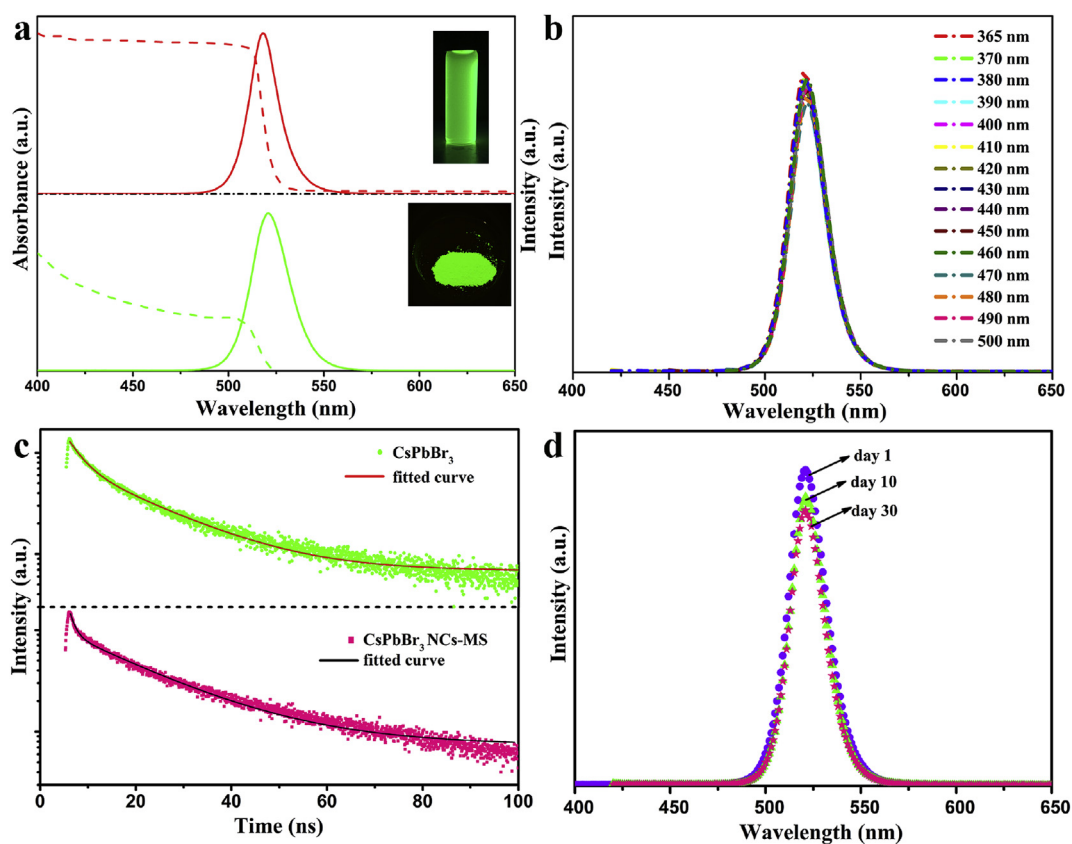


Fig. 5. (a) The absorption (dashed line) and PL (solid line) spectra of the CsPbBr<sub>3</sub> NCs in solution and the as-prepared NCs-MS nanocomposite. (b) PL spectra recorded under the excitation of diverse wavelength lights ranging from 365 to 500 nm. (c) Time-resolved PL decay curves of solution and NCs-MS. (d) PL spectra of the NCs-MS exposed to ambient air. Inset of (a): images of NCs in solution and NCs-MS under UV light.

[36,37]. As shown in Fig. 5d, the PL emission position and shape of NCs-MS nanocomposite did not show significant change under ambient condition for one month, which indicate that NCs-MS nanocomposite have outstanding stability in ambient condition. Therefore, NCs-MS nanocomposite not only exhibits outgoing fluorescence performance but also presents good stability.

To some extent, the thermal quenching of luminescence is also an important parameter to evaluate the performance of optical materials. Normally, the PL intensity gradually decreases with an increase in temperature, which is the universal properties in optical materials due to the enhanced probability of nonradiative transition at high temperature [13]. As shown in Fig. 6a and b and insets, we used a thermal controller system to test the thermal stability. When the temperature ranged from 298 K to 398 K, the relative intensity of the NCs-MS nanocomposite was decreased to 35%, which was higher than that of the CsPbBr<sub>3</sub> NCs, which is owing to oxidation of the NCs surface is suppressed even at elevated temperature after silica coating. The result demonstrated that the as-prepared NCs-MS nanocomposite exhibit much better thermal stability than CsPbBr<sub>3</sub> NCs. Moreover, a photostability test of the NCs-MS nanocomposite and CsPbBr<sub>3</sub> NCs were implemented under continuous UV-light (365 nm) irradiation. In Fig. 6c, after 120 h, the relative intensity of CsPbBr<sub>3</sub> NCs was decreased to about 40%. Because the NCs only have a core structure, which is easily exposed to oxygen and thus causes surface defects. However, the emission intensity of NCs-MS nanocomposite was approximately equal to 80% of the initial intensity. In a further experiment, Fig. 6d demonstrated the PL QY of NCs-MS nanocomposite under an excitation wavelength of 365 nm with the increasing maintenance time in air condition. Clearly, the PLQY of NCs-MS nanocomposite was measured as 46.2%, and after 120 h, the

PLQY decreased to 38%, which indicate NCs-MS nanocomposite show long-term stability. Generally, the NCs only have a core structure, which is easily exposed to oxygen condition and thus causes surface defects. The mesoporous silica shell can act as a protective shell for the core of CsPbBr<sub>3</sub> NCs. The water resistance of NCs-MS nanocomposite was investigated by placing it in an aqueous solution. As shown in the inset of Fig. 6d, the NCs-MS nanocomposite still emit strong green light in water even after 3 h, whereas CsPbBr<sub>3</sub> NCs was almost completely degraded after 20 s. As already mentioned above, NCs-MS nanocomposite exhibit better thermal stability and photostability.

To further investigate the potential application of NCs-MS nanocomposite, a WLED was fabricated by combining green-emitting NCs-MS nanocomposite and red-emitting Sr<sub>2</sub>Si<sub>5</sub>N<sub>8</sub>:Eu<sup>2+</sup> (SSN:Eu<sup>2+</sup>) phosphor with blue InGaN chip. Additionally, considering the heat generated by the blue chips, an effective way to avoid the temperature effect was adopt. That is the remote phosphor configuration in which the phosphor layer is separated from blue chips. In this way, phosphor layer receive much less heat released from the chips owing to the appreciable distance between phosphor and blue chips. Fig. 7a presents the EL spectra of the NCs-MS nanocomposite and red SSN:Eu<sup>2+</sup> phosphor on a blue InGaN chip for generate white light. Obviously, three emission peaks can be seen, which are attributed to the blue chip, green NCs-MS nanocomposite and red SSN:Eu<sup>2+</sup>, respectively. Under the current of 20 mA, the working WLED was shown inset of Fig. 7b and exhibited excellent optical parameters with luminous efficiency (LE) of 47.6 lm/W and color rendering index (CRI) 72.3, the chromaticity coordinates and corrected color temperature (CCT) of the WLED were (0.3365, 0.3390) and 5318 K. In addition, with increasing ratio of SSN:Eu<sup>2+</sup> phosphor, the CIE color

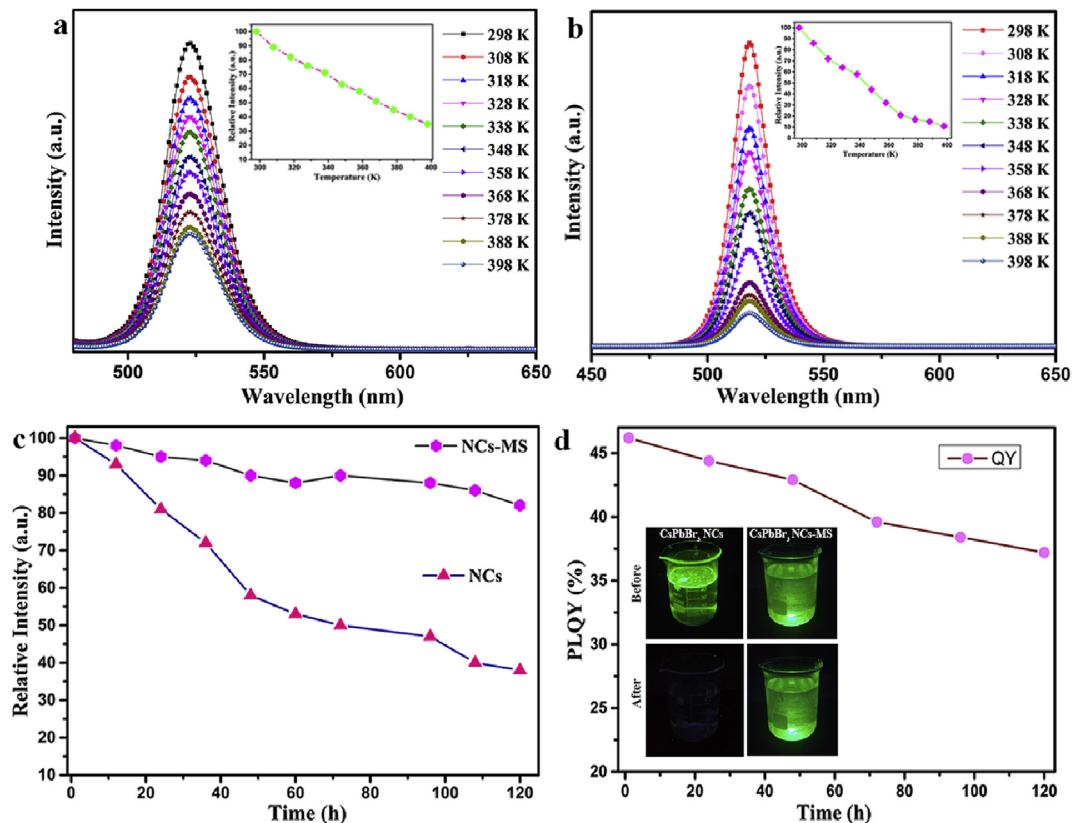


**Fig. 6.** Temperature-dependent PL spectra of (a) CsPbBr<sub>3</sub> NCs-MS nanocomposite and (b) pure CsPbBr<sub>3</sub> NCs in the temperature range of 298–398 K, inset: the relative intensity as a function of temperature in (a) CsPbBr<sub>3</sub> NCs-MS nanocomposite and (b) pure CsPbBr<sub>3</sub> NCs; (c) Photostability test of the NCs-MS and pure CsPbBr<sub>3</sub> NCs. (d) The PLQY stability of the NCs-MS nanocomposite; inset: images of NCs-MS nanocomposite and CsPbBr<sub>3</sub> NCs before and after immersion in aqueous solution.

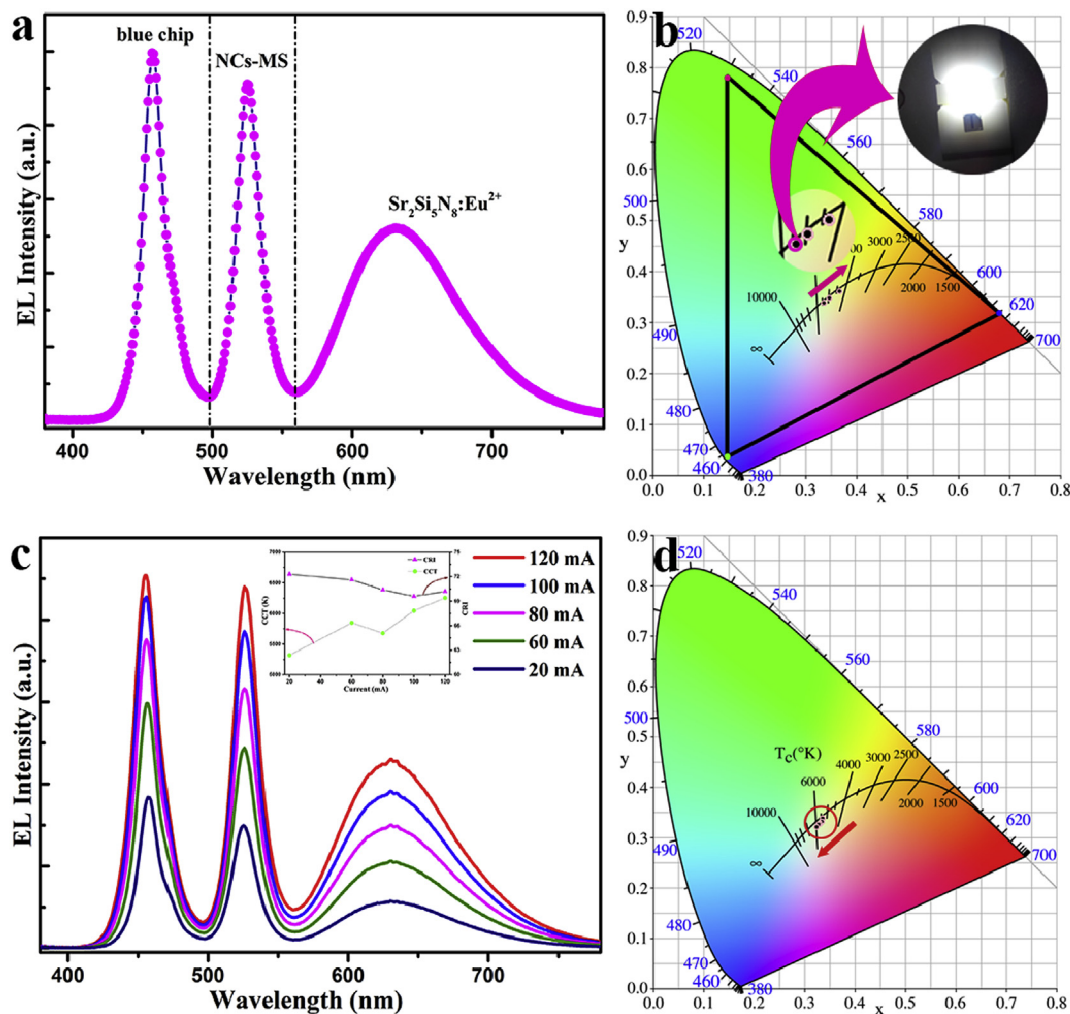


**Fig. 7.** (a) EL spectra of the WLED using the green-emitting NCs-MS nanocomposite and red-emitting Sr<sub>2</sub>Si<sub>5</sub>N<sub>8</sub>:Eu<sup>2+</sup> phosphor. (b) CIE color coordinates of the WLED with device ratios of NCs-MS nanocomposite and Sr<sub>2</sub>Si<sub>5</sub>N<sub>8</sub>:Eu<sup>2+</sup>, the inset shows the photograph of the white light. (c) EL spectra of the WLED under different driving currents ranging from 20 to 120 mA, inset shows the CCT and CRI at different currents. (d) CIE color coordinates of the WLED at different currents. (For interpretation of the references to colour in this figure legend, the reader is referred to the web version of this article.)

coordinates shift to warm white area (Fig. 7b). To evaluate the color stability of this WLED device, the EL spectra of the fabricated WLEDs under different current were investigated and shown in Fig. 7c. With increasing the current from 20 to 120 mA, the LE decreased from 47.6 lm/W to 12.9 lm/W. The decrease of LE is because of the application of the green-emitting NCs-MS nanocomposite and thermal degradation in LED application when used for the generation of white light. The inset of Fig. 7c demonstrated the variation of both CCT and CRI with increasing the current. Clearly, the CCT consequently increased from 5318 to 6253 K, while the CRI decreased from 72.3 to 70.2. Moreover, the corresponding CIE chromaticity coordinates was shown in Fig. 7d, as we can see, the CIE chromaticity coordinates are found slightly shifted to blue from (0.3365, 0.3390) to (0.3247, 0.3215). These results demonstrate that the WLED has excellent color stability. As a consequence, although NCs-MS nanocomposite are weak under a high current density, the practical feasibility of white light generation as down-conversion WLEDs is investigated.

#### 4. Conclusions

In summary, we reported a simple and efficient method to prepare

highly green luminescent and stable CsPbBr<sub>3</sub> NCs-MS nanocomposite, which was fabricated using CsPbBr<sub>3</sub> NCs incorporated into mesoporous silica, for white light generation in optoelectronic devices. The resultant NCs-MS nanocomposite showed excellent optical performance and a narrow emission width. Additionally, compared to the pure CsPbBr<sub>3</sub> NCs, the formed NCs-MS nanocomposite is resistant to water, thereby significantly prolonged lifetime of light emitters in ambient air conditions. More importantly, NCs-MS nanocomposite also exhibited much better thermal stability and photostability. Benefiting from the remarkable optical performance, NCs-MS nanocomposite is a potential candidate with high desirable characteristic for both lamp and display technology. Therefore, WLED were constructed by combining blue InGaN chip with the green-emitting NCs-MS nanocomposite and the red SSN:Eu<sup>2+</sup> phosphors, which demonstrated an outstanding LE of 47.6 lm/W, CRI of 72.3, CCT of 5318 K, as well as excellent-quality white light with CIE color coordinates of (0.3365, 0.3390) under an operating current of 20 mA. It is worth pointing out that the WLED has good color stability when the operational current increases to 120 mA. The abovementioned results indicate that the CsPbBr<sub>3</sub> NCs-MS nanocomposite can be a new luminescent materials in optoelectronic devices.

## Acknowledgements

This study was financially supported by the National Natural Science Foundation of China (51472183 and 51672192).

## References

- [1] X. Li, F. Cao, D. Yu, J. Chen, Z. Sun, Y. Shen, Y. Zhu, L. Wang, Y. Wei, Y. Wu, H. Zeng, *Small* 13 (2017) 1603996.
- [2] Y. Zhang, J. Liu, Z. Wang, Y. Xue, Q. Ou, L. Polavarapu, J. Zheng, X. Qi, Q. Bao, *Chem. Commun.* 52 (2016) 13637–13655.
- [3] M. Chen, Y. Zou, L. Wu, Q. Pan, D. Yang, H. Hu, Y. Tan, Q. Zhong, Y. Xu, H. Liu, B. Sun, Q. Zhang, *Adv. Funct. Mater.* 27 (2017) 1701121.
- [4] L. Protesescu, S. Yakunin, M.I. Bodnarchuk, F. Krieg, R. Caputo, C.H. Hendon, R.X. Yang, A. Walsh, M.V. Kovalenko, *Nano Lett.* 15 (2015) 3692–3696.
- [5] D. Amgar, A. Stern, D. Rotem, D. Porath, L. Etgar, *Nano Lett.* 17 (2017) 1007–1013.
- [6] F.D. Stasio, M. Imran, Q.A. Akkerman, M. Prato, L. Manna, R. Krahne, *J. Phys. Chem. Lett.* 8 (2017) 2725–2729.
- [7] X. Chen, H. Hu, Z. Xia, W. Gao, W. Gou, Y. Qua, Y. Ma, *J. Mater. Chem. C* 5 (2017) 309–313.
- [8] J.P. Park, T.K. Lee, S.K. Kwak, S.W. Kim, *Dyes Pigments* 144 (2017) 151–157.
- [9] J. Li, L. Xu, T. Wang, J. Song, J. Chen, J. Xue, Y. Dong, B. Cai, Q. Shan, B. Han, H. Zeng, *Adv. Mater.* 29 (2017) 1603885.
- [10] Y.H. Song, J.S. Yoo, B.K. Kang, S.H. Choi, E.K. Ji, H.S. Jung, D.H. Yoon, *Nanoscale* 8 (2016) 19523–19526.
- [11] X. Zhang, C. Sun, Y. Zhang, H. Wu, C. Ji, Y. Chuai, P. Wang, S. Wen, C. Zhang, W.W. Yu, *J. Phys. Chem. Lett.* 7 (2016) 4602–4610.
- [12] J. Song, J. Li, X. Li, L. Xu, Y. Dong, H. Zeng, *Adv. Mater.* 27 (2015) 7162–7167.
- [13] D. Chen, Z. Wan, X. Chen, Y. Yuan, J. Zhong, *J. Mater. Chem. C* 4 (2016) 10646–10653.
- [14] Z. Wei, A. Perumal, R. Su, S. Sushant, J. Xing, Q. Zhang, S.T. Tan, H.V. Demir, Q. Xiong, *Nanoscale* 8 (2016) 18021–18026.
- [15] X. Zhang, W. Wang, B. Xu, S. Liu, H. Dai, D. Bian, S. Chen, K. Wang, X.W. Sun, *Nano Energy* 37 (2017) 40–45.
- [16] F. Hu, C. Yin, H. Zhang, C. Sun, W.W. Yu, C. Zhang, X. Wang, Y. Zhang, M. Xiao, *Nano Lett.* 16 (2016) 6425–6430.
- [17] A. Swarnkar, R. Chulliyil, V.K. Ravi, M. Irfanullah, A. Chowdhury, A. Nag, *Angew. Chem.* 127 (2015) 15644–15648.
- [18] S. Yakunin, L. Protesescu, F. Krieg, M.I. Bodnarchuk, G. Nedelcu, M. Humer, G. De Luca, M. Fiebig, W. Heiss, M.V. Kovalenko, *Nat. Commun.* 6 (2015) 8056.
- [19] F. Palazon, F.D. Stasio, Q.A. Akkerman, R. Krahne, M. Prato, L. Manna, *Chem. Mater.* 28 (2016) 2902–2906.
- [20] X. Zhang, H. Lin, H. Huang, C. Reckmeier, Y. Zhang, W.C. Choy, A.L. Rogach, *Nano Lett.* 16 (2016) 1415–1420.
- [21] J. Hai, H. Li, Y. Zhao, F. Chen, Y. Peng, B. Wang, *Chem. Commun.* 53 (2017) 5400–5403.
- [22] A. Swarnkar, A.R. Marshall, E.M. Sanehira, B.D. Chernomordik, D.T. Moore, J.A. Christians, T. Chakrabarti, J.M. Luther, *Science* 354 (2016) 92–95.
- [23] W. Koh, S. Park, Y. Ham, *ChemistrySelect* 1 (2016) 3479–3482.
- [24] Z. Li, L. Kong, S. Huang, L. Li, *Angew. Chem.* 129 (2017) 1–6.
- [25] A. Loiudice, S. Saris, E. Oveisi, D.T.L. Alexander, R. Buonsanti, *Angew. Chem. Int. Ed.* 56 (2017) 1–7.
- [26] F. Palazon, Q.A. Akkerman, M. Prato, L. Manna, *ACS Nano* 10 (2016) 1224–1230.
- [27] K. Xu, C. Lin, X. Xie, A. Meijerink, *Chem. Mater.* 29 (2017) 4265–4272.
- [28] W. Chen, J. Hao, W. Hu, Z. Zang, X. Tang, L. Fang, T. Niu, M. Zhou, *Small* 13 (2017) 1604085.
- [29] N. Wang, S. Koh, B.G. Jeong, D. Lee, W.D. Kim, K. Park, M.K. Nam, K. Lee, Y. Kim, B.H. Lee, K. Lee, W.K. Bae, D.C. Lee, *Nanotechnology* 28 (2017) 185603–185611.
- [30] C. Sun, Y. Zhang, C. Ruan, C.Y. Yin, X.Y. Wang, Y.D. Wang, W.W. Yu, *Adv. Mater.* 28 (2016) 10088–10094.
- [31] H. Huang, B. Chen, Z. Wang, T.F. Hung, A.S. Susha, H. Zhong, A.L. Rogach, *Chem. Sci.* 7 (2016) 5699–5703.
- [32] L. Peng, J. Geng, L. Ai, Y. Zhang, R. Xie, W. Yang, *Nanotechnology* 27 (2016) 3356041.
- [33] V.K. Ravi, G.B. Markad, A. Nag, *ACS Energy Lett.* 1 (2016) 665–671.
- [34] S. Sun, D. Yuan, Y. Xu, A. Wang, Z. Deng, *ACS Nano* 10 (2016) 3648–3657.
- [35] X. Li, Y. Wu, S. Zhang, B. Cai, Y. Gu, J. Song, H. Zeng, *Adv. Funct. Mater.* 26 (2016) 2435–2445.
- [36] S. Wei, Y. Yang, X. Kang, L. Wang, L. Huang, D. Pan, *Chem. Commun.* 52 (2016) 7265–7268.
- [37] F. Hu, H. Zhang, C. Sun, C. Yin, B. Lv, C. Zhang, W.W. Yu, X. Wang, Y. Zhang, M. Xiao, *ACS Nano* 9 (2015) 12410–12416.